Article

Seeded Growth of Large Gold Nanorods Modulated by Halide-Mediated Kinetics

Francisco Bevilacqua [1,2] and Luis M. Liz-Marzán [1,2,3,4,*]

[1] CIC biomaGUNE, Basque Research and Technology Alliance (BRTA), 20014 Donostia-San Sebastián, Spain
[2] Biomedical Networking Center of Bioengineering, Biomaterials and Nanomedicine, CIBER-BBN, 20014 Donostia-San Sebastián, Spain
[3] Ikerbasque, Basque Foundation for Science, 48009 Bilbao, Spain
[4] CINBIO, University of Vigo, 36310 Vigo, Spain
* Correspondence: llizmarzan@cicbiomagune.es

Received: 24 September 2025; Revised: 23 October 2025; Accepted: 3 November 2025; Published: 4 November 2025

Abstract: We report a robust and versatile method to overgrow pentatwinned gold nanorods using a combination of cetyltrimehylammonium chloride (CTAC) and bromide (CTAB), thereby expanding current protocols to the production of larger nanorod dimensions. When increasing CTAB content in the reaction medium, the aspect ratio of the resulting nanorods was found to decrease, due to the higher binding energy of bromide on gold surfaces, compared to chloride. A further handle to tailor the dimensions of larger nanorods can be achieved by tuning the Au^{3+}/Au^{0} ratio. At a fixed CTAB concentration, increasing Au^{3+}/Au^{0} ratio resulted in larger nanorods with minor variation of the aspect ratio, which again highlights the central role of CTAB in the overgrowth process. Our findings highlight the effect of CTAB on both growth kinetics and facet stabilization, offering a simple approach to finely tune the dimensions of pentatwinned gold nanorods. We also demonstrate the versatile use of CTAB/CTAC ratio in a more standard synthesis method, again leading to fine tuning of nanorod dimensions.

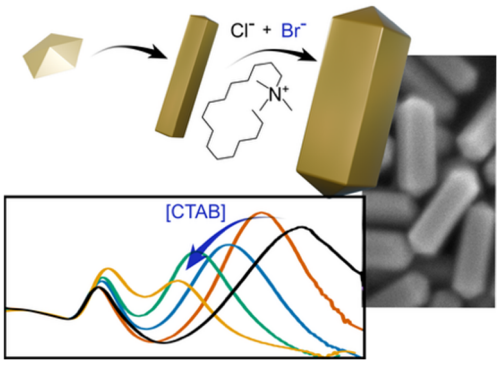

Keywords: gold; nanorods; CTAB; growth mechanism; plasmonic nanoparticles

1. Introduction

Since the early works by Murphy and El-Sayed [1,2], the synthesis of gold nanorods (AuNRs) has been repeatedly optimized and is currently one of the best-established fabrication procedures in nanomaterials research [3–5]. The superior quality of the nanomaterials obtained through these synthetic protocols allows precise tunability in the corresponding localized surface plasmon resonance (LSPR), in turn providing broad applicability in fields such as photothermal therapy, sensing, and imaging, among others [6–8]. The development of reliable synthetic protocols has been enabled by extensive studies of the involved growth mechanisms and detailed understanding of the influence of individual synthetic parameters, leading to a precise control over AuNR dimensions and, consequently, their optical properties [4,5,9,10]. The control over nanoparticle shape is achieved by performing nucleation and growth in separate reaction steps. First, small, quasi-spherical gold nanoparticles are formed by mixing $AuCl_4^-$ in solution with a strong reducing agent, most frequently sodium borohydride. Subsequently, these "seeds" are overgrown by further addition of $AuCl_4^-$, together with shape-directing reagents—quaternary ammonium surfactants, halide counter-ions, and often Ag^+ ions—and a weak reducing agent, usually ascorbic acid (AA). The use of a weak reductant promotes the initial reduction of Au^{3+} to Au^+, while avoiding complete reduction into Au^0 in the absence of seeds [1]. In this manner, reduction of Au^+ into Au^0 only occurs on the surface of the added gold seeds, leading to a more uniform growth and restricting homogeneous nucleation of gold particles. In this growth scheme the crystallinity of the seeds plays a key role in determining the morphology of the fully grown nanorods [4,11].

In broad terms, AuNRs can be synthesized using seeds with two different crystallographic habits, either single-crystalline (SC) [2,5] or pentatwinned (PT) [4,12]. On one hand, SC seeds have no crystal twin defects, and

are commonly employed to prepare single-crystal AuNRs (SC-AuNRs) in the presence of Ag^+ ions. On the other hand, PT seeds contain five twin boundaries, which propagate during (Ag-free) seeded growth, leading to the formation of pentatwinned AuNRs (PT-AuNRs) with 5-fold symmetry along the long axis. However, the formation of PT seeds in high yield has proven challenging and often requires extensive purification steps [12]. Albeit less commonly used than SC-AuNR, PT-AuNR allow the preparation of larger nanoparticles, with the additional advantage that silver is not present in their composition, thus reducing cytotoxicity and facilitating surface conjugation [4,12]. Typically, the preparation of SC-AuNRs requires a growth solution containing—apart from $HAuCl_4$ and AA—a high concentration of the surfactant hexadecyltrimethylammonium bromide (CTAB), HCl, and $AgNO_3$ [2,3,5], whereas PT-AuNRs solely require the presence of CTAB, which is also present in a smaller amount compared to SC-AuNRs. Standard SC-AuNRs are characterized by small dimensions and aspect ratios up to ~8, ranging from "minirods" (~20 nm length and diameter below 10 nm) to larger rods with lengths in the hundred nm range [5,13,14]. On the other hand, PT-AuNRs can be grown into larger dimensions (>100 nm length) and longer aspect ratios >20 [12,15,16]**.** Structurally, SC- and PT-AuNRs exhibit key differences in the Miller indices of their surface facets, which is relevant for various applications and processes, such as catalysis, bioconjugation, self-assembly, or seeded overgrowth: SC-AuNRs expose high-index {520} facets (combined with {100} and {110}) along their sides and a combination of {111}, {100}, and {110} facets at their tips [17]; whereas PT-AuNRs predominantly display low-index {100} lateral facets and {111} tip facets due to the presence of five twin planes that impose a pentagonal cross section [4,18].

The control over anisotropic growth of AuNRs depends on the shape-directing ability of the different reagents, involving effects on the thermodynamic stability of the resulting surface facets and on reaction kinetics. Surfactant molecules have an influence on three key aspects of particle growth: (i) stabilization of nanoparticles to prevent aggregation, (ii) formation of complexes with gold ions and modulation of their reduction potential and kinetics, and (iii) promotion of anisotropic growth by selective facet stabilization. Therefore, understanding their influence on the two latter aspects is crucial to gain control over the dimensions and quality of the resulting particles. Several studies reported the influence of various surfactants and other surface-binding ligands. Among these, CTAB and other quaternary ammonium salts—hexadecyltrimethylammonium chloride (CTAC) and others—have been the subject of extensive investigation [19–21]. These studies have emphasized the importance of the cetyltrimethylammonium (CTA^+) cationic surfactant for directing nanorod growth through two main mechanisms, namely the packing density and the organization of the organic surface layer, both influencing the accessibility of reactants to the Au surface to allow further Au reduction [18,20]. For example, in CTAB-mediated synthesis, CTA^+ molecules exhibit a higher packing density on {100} facets compared to {111} facets [18,20]. Interestingly, "patchy" structures on gold surfaces have been proposed at low CTA^+ concentrations, with more continuous layers at higher concentrations [18,22,23]. On the other hand, studies on CTAC showed weaker CTA^+ adsorption onto gold surfaces, creating a more diffuse surfactant layer that allows easier access to the gold surface [20,23]. An important component of the surfactant is thus the counterion—typically a halide—which plays a major role during anisotropic growth. Bromide ions ($Br^–$) have a higher binding energy to gold surfaces compared to chloride ($Cl^–$), thereby leading to a slower deposition rate of Au^0 on the growing seed facets [17]. Accordingly, the addition of $Br^–$ to the growth solution can be used to increase the local density of CTA^+ on the gold surface [20,24]. Overall, the differences in specific adsorption for CTAB and CTAC explain why CTAB is preferred in syntheses that require kinetic regulation and symmetry breaking [3–5], whereas CTAC is more commonly employed in the synthesis of isotropic nanoparticles [10].

Binary surfactant systems have been investigated for the preparation of high aspect ratio PT-AuNRs from SC seeds. For example, binary surfactant mixtures combining oleic acid and CTAB were employed to achieve high aspect ratio PT-NRs in relatively high yield (>70%) [15]. It is generally understood that a slower gold reduction rate leads to nanorods with higher aspect ratio; this can be achieved by decreasing the reaction pH (i.e., regulating the presence of the ascorbate anions responsible for reduction of Au^{3+} to Au^+), decreasing the concentration of reducing agent, or lowering the reaction temperature [5,24]. However, reducing reaction temperature can be challenging for syntheses employing high CTAB concentrations because of the low solubility of CTAB in water, which spontaneously crystallizes below ~25 °C. Our group has recently demonstrated that a suitable CTAB/CTAC ratio can be selected to enable seeded growth at low temperatures down to 8 °C, thereby expanding the accessible dimensions of PT-AuNRs [24]. We have also reported that the overgrowth of pre-formed PT-AuNRs in the presence of CTAC at 30 °C results in the formation of large PT bipyramids, eventually featuring a thicker equatorial belt [25].

Despite these developments, studies on PT-AuNR synthesis remain scarce compared to SC-AuNRs, for which numerous optimization procedures have been reported, resulting in great reproducibility and control over aspect ratio and dimensions. We thus aimed at identifying suitable conditions to obtain PT-AuNRs with larger dimensions while keeping a low aspect ratio (and LSPR modes within the visible or near-IR). Using pre-formed

PT-AuNRs as seeds, we focused on the role of CTAB in regulating the growth kinetics for different Au^{3+} to seed ratios. We thus hypothesized that, by using CTAB/CTAC surfactant mixtures with different ratios, we would modulate surface accessibility during growth and in turn the deposition of reduced Au atoms. As a result, we developed a robust method to overgrow pre-formed PT-AuNRs into larger PT-AuNRs with tunable aspect ratio, which we demonstrate for nanorods with dimensions (length × width) ranging from 126 nm × 60 nm to 266 nm × 76 nm. We additionally demonstrate that, by tailoring the CTAB/CTAC ratio, AuNR dimensions could also be tuned for PT-AuNRs grown from small PT seeds [24], thus offering a general strategy to tune the aspect ratio and expand the accessible sizes of PT-AuNRs.

2. Materials and Methods

2.1. Materials

Analytical grade reagents, $HAuCl_4 \cdot 3H_2O$ (≥99.9%), L-ascorbic acid (99%), cetyltrimethylammonium bromide (CTAB, ≥96.0%), cetyltrimethylammonium chloride (CTAC, 25 wt% in H_2O), citric acid (≥99.5%), sodium borohydride (≥99.0%), were all purchased from Merck, Darmstadt, Germany.

2.2. Preparation of pentatwinned seeds

PT Au seeds were prepared following a previously reported protocol [4]. Typically, 5 mL of 100 mM CTAC was first mixed with 0.5 mL of 100 mM citric acid and 4.2 mL of water. Subsequently, 50 µL of 50 mM $HAuCl_4$ was added under stirring. The solution was left under mild magnetic stirring (200–300 rpm) for 30 min to ensure homogeneous mixing. After this time, 250 µL of a freshly prepared ice-cold 25 mM $NaBH_4$ solution was quickly added under vigorous stirring (>1000 rpm) the color turned from light yellow to light brown. At this stage, a UV-vis spectrum was recorded to verify gold salt reduction through the absorbance at 400 nm (the value should be close to 0.6 for an optical pathlength of 1 cm). After borohydride addition, the solution was kept at room temperature for 15 min to ensure borohydride decomposition, followed by a heat treatment at 80 °C for 90 min, during which the color of the solution turned red. A larger amount of borohydride might result in extensive overgrowth during the heat treatment and thus a lower yield of twinning. At this stage the spectrum can be checked, and the peak should be below 529 nm; above this value no twinning could be observed.

2.3. Growth of 113 nm × 26 nm Au pentatwinned nanorods

The preparation of PT-AuNRs was based on the protocol reported in the same study as the PT seeds [4]. A 100 mL solution of 8 mM CTAB was prepared, to which 250 µL of 50 mM $HAuCl_4$ was added. The solution was left for 15 min under mild magnetic stirring to ensure the formation of [Br-Au-Br] complexes, followed by 15 additional minutes in a water bath at 20 °C. Thereafter, 250 µL of 100 mM AA solution and 230 µL of PT seeds were added under vigorous stirring. The solution was subsequently stored at 20 °C overnight without stirring. After synthesis, the obtained nanorods were centrifuged at 6,500 rpm for 15 min and redispersed in CTAC 100 mM. The particles were finally redispersed in 2 mL of MilliQ water, with a concentration (estimated from the absorbance at 400 nm) of 2.67 mM Au^0. A representative TEM image and UV-vis-NIR spectrum are shown in Figure S1. Statistical analysis from over 100 particles yielded average dimensions of 113 ± 6 nm in length, 26 ± 2 nm in width, and aspect ratio of 4.4 ± 0.5.

2.4. Overgrowth of PT-AuNRs

Typically, a 10 mL solution of 25 mM CTAC and a given concentration of CTAB was prepared by mixing 2.5 mL of 100 mM CTAC solution and the corresponding volume of a 100 mM CTAB solution and storing at 30 °C. To this mixed solution, 20 µL of 50 mM $HAuCl_4$ was added under mild stirring (200–300 rpm) and left for 15 min to stabilize the temperature. After 15 min, 20 µL of 100 mM AA and a selected amount of PT-AuNR seeds (see Tables S1 and S2) were added under vigorous stirring (700–800 rpm). The reaction was left to proceed at 30 °C under mild stirring for either 90 min ([CTAB] = 0.5–2 mM) or 2 h ([CTAB] = 5–10 mM). After this time, the particles were centrifuged at 2500 rpm for 8 min. The supernatant was discarded, and particles were redispersed in 2 mL of miliQ water.

2.5. Kinetic study

After the addition of gold salt in the reaction medium—initiation of the reaction, t_0—1 mL of the reaction mixture was poured in a plastic semi-microcuvette (1 cm path length) in the spectrometer holder, which was

connected to a water bath for temperature regulation at 30 °C. A spectrum was registered every 2 min for the first 10 min, then at 15 min, 20 min, and finally every 10 min for the remaining time of the reaction.

2.6. Growth from PT seeds

The growth of PT-AuNRs from PT seeds was adapted from a previously reported protocol [24]. Three 10 mL solutions of 100 mM CTAC containing, 4 mM CTAB, 6 mM CTAB, and 8 mM CTAB, were first prepared, to which 25 μL of 50 mM $HAuCl_4$ was added. The solutions were stirred for 15 min, and then placed in a water bath at 8 °C for 30 min. After this time, 25 μL of 100 mM AA was added, followed by 25 μL of PT seeds, both under vigorous stirring (700–800 rpm). After 90 min, the samples were centrifuged and purified by depletion separation using 100 mM CTAC, overnight. The pink supernatant was discarded and the particles were dispersed in 1 mL of miliQ water.

2.7. Optical characterization

Spectroscopic characterization was conducted with an Agilent 8453 UV−vis−NIR diode array spectrophotometer (Agilent Santa Clara, CA, USA) in the 350–1100 nm wavelength range. Typically, after synthesis, the particles were centrifuged (at 2500 rpm for 8 min), then redispersed in milliQ water and placed in a polystyrene cuvette (1 cm path length).

2.8. Electron microscopy

Transmission electron microscopy (TEM) images were captured with a JEOL JEM-1400PLUS (Tokyo, Japan) transmission electron microscope operating at 120 kV. Scanning electron microscopy (SEM) images were acquired using a JSM-IT800HL from JEOL (Tokyo, Japan) equipped with a secondary electron detector (SED) using 3–5 kV, under high vacuum.

2.9. Yield and measurement details

The yield in shape purity was estimated by counting 400–500 particles per sample. The particles were separated into three categories: “rods”, corresponding to pointy rods as the main product of the synthesis; “defective rods”, which exhibited anisotropy but with defects such as dumbbell shapes or protuberances; “non-rods” corresponding to the remaining minority shapes, as indicated in Tables S1 and S2. More than 150 particles were measured from each sample to determine the average length, width, and side length, as illustrated in Figure S2. Details on estimation of particle volume are provided in the Supporting Information.

3. Results and Discussion

On the basis of our previous experience in the growth of PT-AuNRs into large bipyramids [25], we first synthesized PT-AuNR seeds 113 ± 6 nm, 26 ± 2 nm (in short, 113 nm-PT-AuNRs) (Figure S1) using a previously reported protocol (see Section 2) [4]. In a first attempt, AA and 113 nm-PT-AuNR seeds were incubated with CTAC 25 mM and different CTAB concentrations, at 30 °C for 15 min, followed by addition of $HAuCl_4$ under vigorous stirring and allowing the reaction to proceed for 90 min. A summary of the obtained products using both 0.5 mM and 1 mM CTAB is presented in Figure S3. Although the obtained particles displayed a rod-like morphology, TEM images revealed a non-negligible proportion of dumbbell-like or defective rods. Therefore, we proceeded to alter the order of addition of reactants, to ensure complete pre-reduction of Au^{3+} into Au^{+}. The improved overgrowth procedure involved first mixing $HAuCl_4$ with a solution containing CTAC (25 mM) and selected concentrations of CTAB (0.5–10 mM), under mild stirring (200 rpm) at 30 °C for 15 min, followed by addition of AA and 113 nm PT-AuNR seeds, under vigorous stirring (800–1000 rpm). Thanks to this pre-reduction step, the quality of the products was significantly improved, with a yield of well-defined PT-AuNRs over 98% (see Figure S3). However, we found the AA/Au^{3+} ratio to have a moderate impact on the dimensions and quality of the final particles (Figure S4).

After establishing a reliable overgrowth protocol, we aimed at exploring the impact of CTAB concentration, keeping all other reagent concentrations constant, including an Au^{3+}/Au^{0} ratio = 12.5. The well-defined (longitudinal and transverse) LSPR modes in AuNRs allow for a quick initial characterization of seeded growth, simply by recording UV-Vis-NIR spectra of the prepared colloidal dispersions. The spectra for samples prepared at constant seed concentration and Au^{3+}/Au^{0} ratio, but varying CTAB/CTAC ratio (by increasing CTAB concentration) are displayed in Figure 1a. The position of the longitudinal LSPR peak exhibits a gradual blue shift (from 940 to 680 nm) for particles overgrown in the presence of increasing CTAB concentrations, as well as a relative increase in the

intensity of the transverse LSPR band. The corresponding TEM images (Figure 1b–f) reveal the formation of AuNRs with dimensions ranging from 203 nm × 66 nm to 145 nm × 84 nm, as CTAB concentration was increased (see histograms in Figure S5). The geometrical features measured from TEM images are summarized in Table S1 and confirm that the observed longitudinal LSPR blue shift correlates with a gradual decrease in aspect ratio, as expected for AuNRs [26]. Moreover, the small standard deviations in length and width reveal a low polydispersity (<10%) in all cases. Complementary scanning electron microscopy (SEM) measurements were conducted to unveil more detailed morphological features (Figures 1g,h and S6). SEM images evidence the presence of sharp tips on the obtained PT-AuNRs, with a well-defined pentagonal cross-section and sharp faceting. SEM analysis further confirms the low polydispersity of the samples produced. Finally, we demonstrate the feasibility of scaling the synthesis up to a total volume of 100 mL, using 5 mM CTAB. The produced particles showed high homogeneity in both shape and size (<10%), thus confirming the robustness of the synthesis protocol and potential upscaling to even larger volumes with no loss of sample quality (see Figure S7).

For consistency, we carried out optical simulations based on a quasi-analytical model for selected geometries [27]. We selected a cylindrical rod model for AuNRs with the average dimensions of our PT-AuNRs, as determined by TEM (Figure S8 and Table S1). The simulated spectra follow the same trend as the experimental ones, not only in the LSPR position, but also in the increased intensity of the transverse mode. However, the precise position of the LSPR band exhibits some discrepancies, which are minor for the samples obtained with [CTAB] ranging from 2 to 10 mM (~10–20 nm), but higher for the lowest CTAB concentration (~50 nm). Overall, these differences between experimental and simulated data are consistent among samples, supporting the idea that they are mainly due to the geometrical differences between the actual particles (pentagonal prisms with sharp tips) and the model (cylinder with hemispherical tips). However, the largest observed difference (50 nm for the 0.5 mM CTAB sample) suggests that the influence of these morphological features on the optical activity of the particles becomes more relevant for more elongated particles.

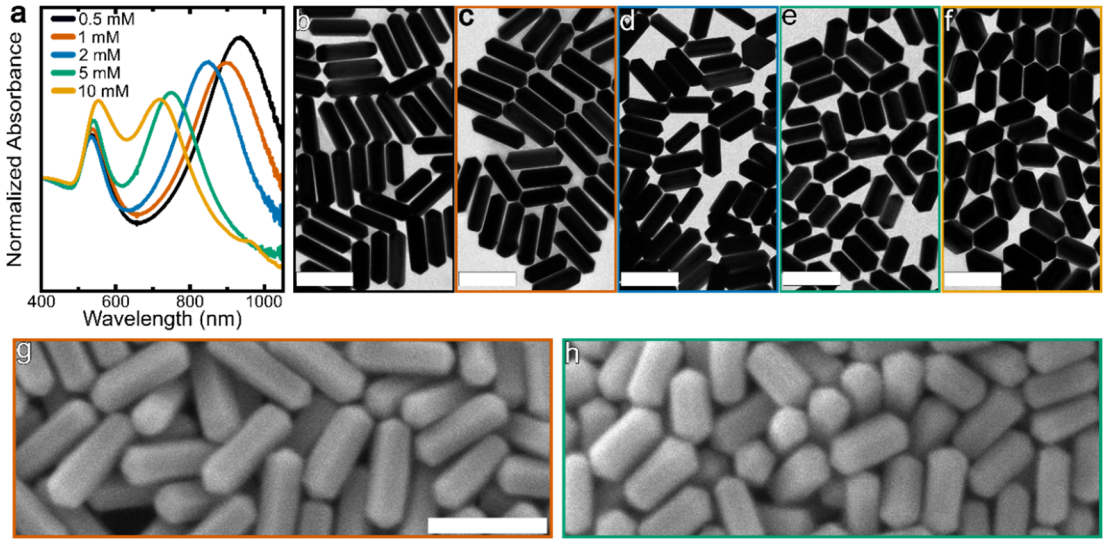

Figure 1. Overgrowth of PT-AuNRs at constant Au^{3+}/Au^0 = 12.5 and [CTAC] = 25 mM, with varying [CTAB] from 0.5 to 10 mM. (**a**) UV-vis-NIR spectra (normalized at 400 nm) for nanorods grown from 113 nm-PT-AuNR seeds at different CTAB concentrations. (**b**–**f**) TEM micrographs corresponding to the spectra in (**a**), with CTAB concentrations of 0.5 mM ((**b**), 202 nm × 60 nm), 1 mM ((**c**), 203 nm × 66 nm), 2 mM ((**d**), 171 nm × 70 nm), 5 mM ((**e**), 154 nm × 71 nm), and 10 mM ((**f**), 145 nm × 84 nm). SEM images of Pt-AuNRs obtained by seeded growth from 113 nm-PT-AuNR using Au^{3+}/Au^0 = 12.5 and different CTAB concentrations of 1 mM (**g**) and 5 mM (**h**). All scale bars represent 200 nm; the scale bar in (**g**) is also valid for (**h**).

To further assess the robustness of the synthesis, we estimated the average volume of the synthesized NRs using the calculation outlined in the Supporting Information (see Figure S2). Because a constant Au^{3+}/Au^0 ratio and PT-AuNR seed concentration were maintained for all syntheses with different CTAB concentrations, the initial AuNRs should have grown by the same proportion, and the final particles should reach approximately the same volume. The results are shown in Table S1 and confirm this hypothesis, albeit with minor deviations, from ~4% to ~15% for the 5–0.5 mM and 5–10 mM ranges, respectively. Although a 15% deviation lies slightly above the standard deviation of the sample dimensions (~10%), this difference may arise from deviations from the regular pentagonal cylinder geometry for some deformed nanorods. Overall, the synthesis proved to be effective and reproducible, resulting in high-quality nanorods at any of the selected CTAB concentrations.

We next employed UV-vis-NIR spectroscopy to investigate the effect of CTAB concentration on the kinetics of AuNR overgrowth. Two effects were expected from an increase in the concentration of CTAB in solution, namely an increase of the CTA^+ density at the AuNR surface and a higher density of bromide ions adsorbing on the gold surface, both effects contributing to a slower reduction and deposition of gold atoms [18,23]. Additionally, the CTA^+ and Br^- densities are also expected to be higher on {100} facets, thereby stabilizing them and favoring growth on {111} facets [20]. Shown in Figure 2a–e are the spectral traces during overgrowth, using an Au^{3+}/Au^0 ratio of 12.5, for the different CTAB concentrations, from 0.5 mM to 10 mM. During the overgrowth process, a spectrum was acquired every 2 min for the first 10 min (grey), followed by spectra at 15 and 20 min (brown), and then one spectrum every 10 min (green) until the absorbance at 400 nm reached a plateau. This strategy allowed us to identify differences in the growth rate, from the variations in both absorbance and LSPR position. The absorbance at 400 nm (mostly contributed by interband transitions in metallic gold [28]) can be used as a qualitative indicator of the reduction of Au^+ to Au^0. It should however be noted that, in the case of large nanoparticles, a significant contribution of scattering is expected, which hinders a quantitative analysis using this parameter [29]. Thus, to facilitate analysis of the kinetics we plotted in Figure 2f the absorbance at 400 nm as function of time. These plots clearly show differences in the initial increase of absorbance, as the slope decreases with increasing CTAB concentration. Moreover, a longer time is required for the absorbance to reach a plateau in the case of the higher CTAB concentrations (120 min for 10 mM CTAB versus 50 min for 0.5 mM CTAB). The time evolution of the longitudinal LSPR maximum is more complex (see Figure S9) because of the relative contributions of absorption and scattering during the morphological evolution of the NRs. These kinetic experiments confirmed the expected impact of Br^-, and CTA^+ on gold reduction kinetics, in agreement with previous literature reports [18,20,23].

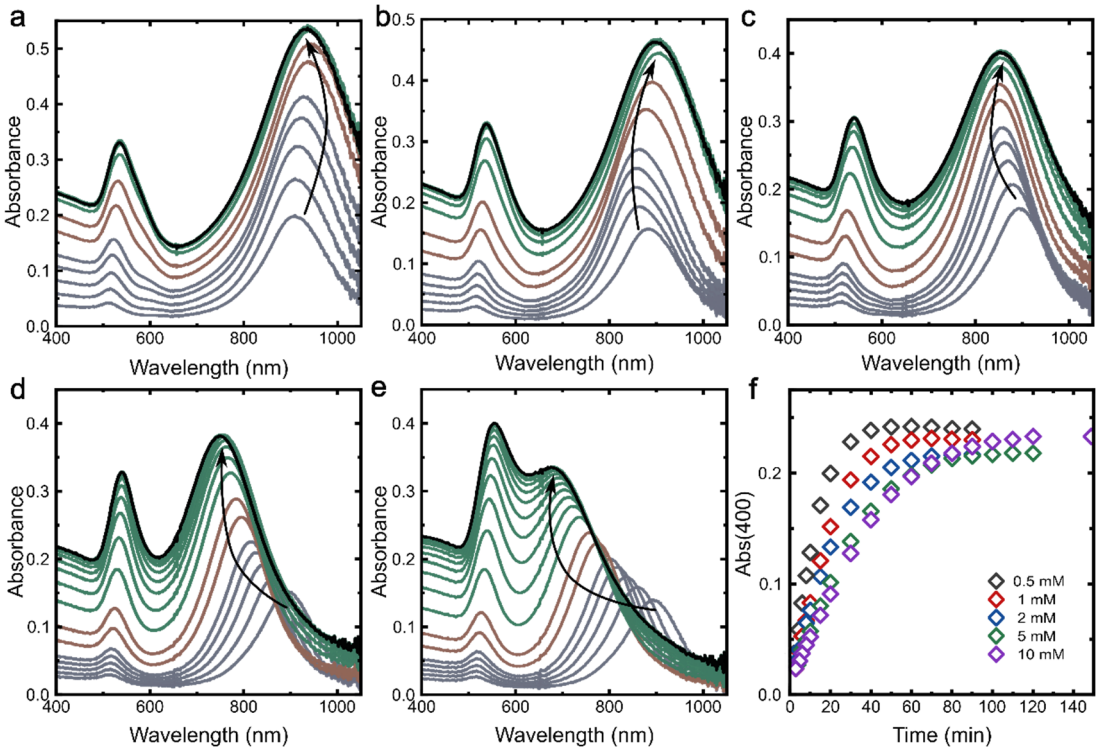

Figure 2. Effect of CTAB concentration on overgrowth kinetics. Spectral evolution during the overgrowth of 113 nm-PT-AuNRs using Au^{3+}/Au^0 = 12.5, for different CTAB concentrations: 0.5 mM (**a**), 1 mM (**b**), 2 mM (**c**), 5 mM (**d**), and 10 mM (**e**). A UV-vis-NIR spectrum was acquired every 2 min for the first 10 min (grey lines), then at 15 min, 20 min (brown), and every 10 min (green). (**f**) Evolution of the absorbance at 400 nm during the overgrowth of 113 nm-PT-AuNRs, as a function of CTAB concentration. Arrows are a guide for the eye showing the LSPR shift.

Aiming at a further range of particle dimensions, we carried out overgrowth experiments at constant CTAB concentrations, but increasing the Au^{3+}/Au^0 ratio (Figure 3). In all cases, when decreasing seed concentration in the growth solution, a red shift was observed in the longitudinal LSPR band, which should be related to an increase in aspect ratio [26]. The average dimensions for the different samples, obtained from TEM measurements are listed in Table S2. When using 0.5 mM CTAB, a small increase in aspect ratio was observed, from 3.28 to 3.47, a difference

that was within the standard deviations. Similarly, the aspect ratios for other samples were not found to show a clear increase or decrease, consistently remaining within the standard deviation range. For example, at 1 mM we observed a maximum aspect ratio of 2.98 at Au^{3+}/Au^0 = 18.75, and a smaller aspect ratio of 2.78 at Au^{3+}/Au^0 = 6.25. On the other hand, at the higher CTAB concentrations—5 mM and 10 mM—the aspect ratio appeared to slightly decrease for higher Au^{3+}/Au^0 ratios, but again remaining within the range of the standard deviation. Thus, we hypothesize that, under these synthetic conditions, the influence of CTAB concentration on the overgrowth process largely defines the aspect ratio, whereas the Au^{3+}/Au^0 ratio affects the final dimensions but not the aspect ratio. These optical changes were again supported by theoretical modeling using the cylindrical NR model, as shown in Figure S10, Table S2. Additionally, estimations of the average volume for the various samples was carried out to confirm complete overgrowth. As summarized in Figure S11, the values obtained for the volumes are within a narrow range for each Au^{3+}/Au^0 ratio and a high R^2 value of 0.99 was determined in a linear regression through the values for different Au^{3+}/Au^0 ratios, evidencing a linear evolution of rod volume as expected.

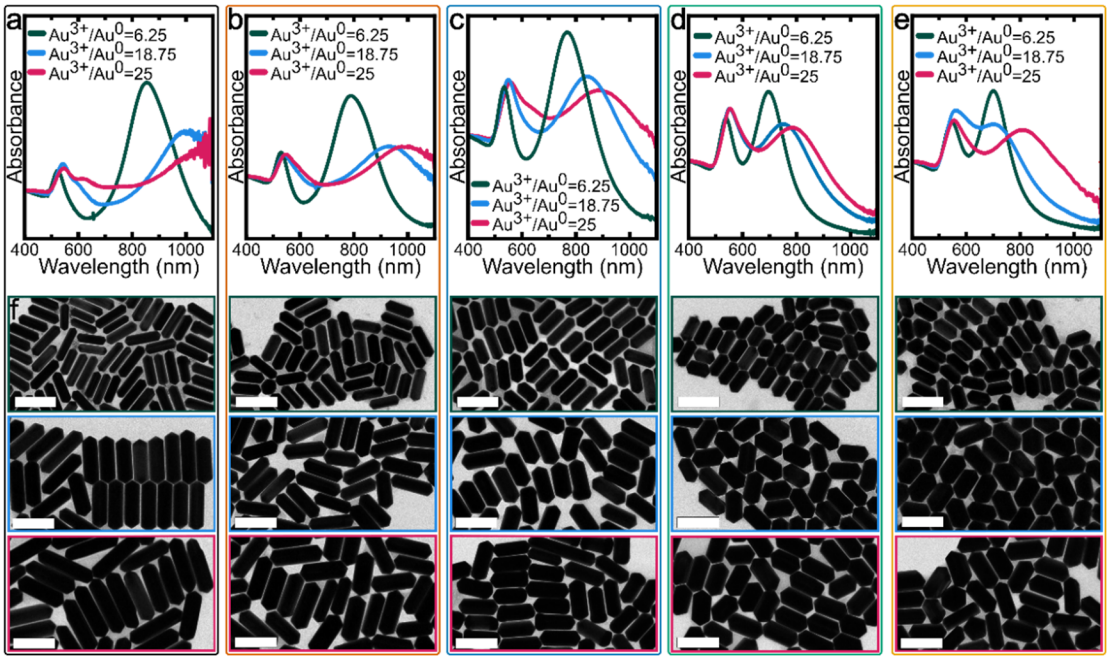

Figure 3. Study of the effect of Au^{3+}/Au^0 at different [CTAB] = 0.5 mM–10 mM. The top row shows UV-vis-NIR spectra for the produced particles using [CTAB] = 0.5 mM (**a**), 1 mM (**b**), 2 mM (**c**), 5 mM (**d**), and 10 mM (**e**). All spectra were normalized at 400 nm. (**f**) TEM micrographs are shown for the particles prepared using Au^{3+}/Au^0 ratios of 6.25 (**upper row**), 18.75 (**middle row**), and 25 (**bottom row**), for every CTAB concentration. All scale bars are 200 nm.

Finally, we aimed to demonstrate the general application of CTAB concentration as a versatile parameter for modulation of growth kinetics and dimensions of PT-AuNRs. Therefore, we investigated the effect of CTAB concentration on a previously reported low-temperature synthesis protocol, using small decahedral seeds (see Section 2) [24]. The reported protocol was previously optimized for a mixture of 2 mM CTAB and 100 mM CTAC. To show the versatility of the CTAB modification method, we simply varied CTAB concentration within the same protocol, carrying out the reaction at 8 °C. The results obtained for PT-AuNRs prepared in the presence of 4 mM, 6 mM, and 8 mM CTAB are summarized in Figure 4. UV-vis-NIR spectra showed the expected blue shift of the longitudinal LSPR band while increasing CTAB concentration, from 958 to 867, and finally 831 nm, for 4, 6, and 8 mM, respectively. Accordingly, TEM characterization of the resulting nanorods revealed a gradually smaller aspect ratio, arising from the following dimensions, 134 ± 10 nm × 28 ± 1 nm (AR 4.8 ± 0.4) for 4 mM CTAB, 122 ± 9 nm × 31 ± 1 nm (AR 3.8 ± 0.4) for 6 mM CTAB, and 114 ± 8 nm × 32 ± 2 nm (AR 3.6 ± 0.4) for 8 mM CTAB.

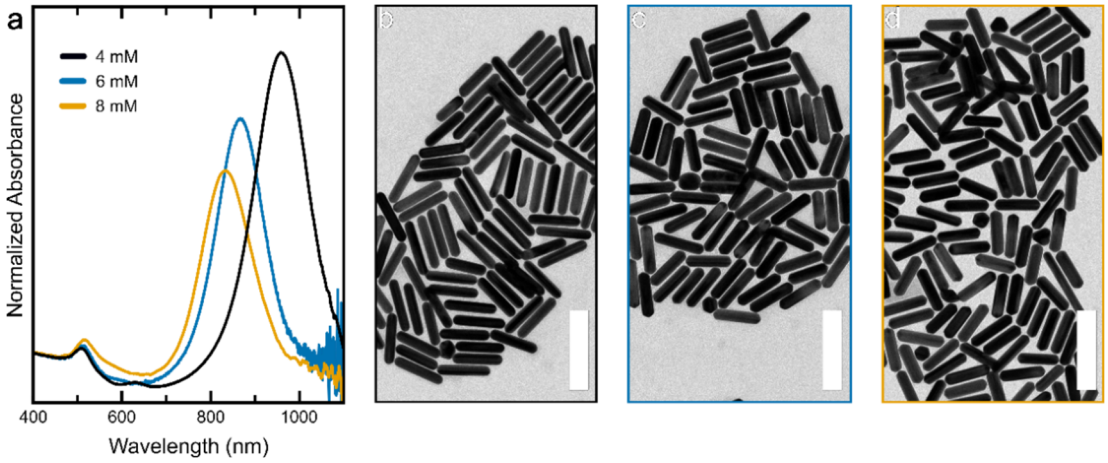

Figure 4. Application of CTAB-induced modulation of PT-AuNR growth from small PT Au seeds [24]. (**a**) Normalized UV-vis-NIR spectra of nanorods prepared using 4 mM, 6 mM, and 8 mM CTAB with $Au^{3+}/Au^{0} = 200$. TEM micrographs of the corresponding products for 4 mM (**b**), 6 mM (**c**), and 8 mM (**d**) CTAB. Spectra are normalized at 400 nm; scale bars are 200 nm.

4. Conclusions

The ratio between bromide and chloride counter-ions can be used to modulate the shape-directing effect of quaternary ammonium surfactants. By using a combination of CTAC and CTAB, the overgrowth of pre-formed PT-AuNRs can be tuned for the preparation of larger nanorods (up to several hundred nm), while maintaining the high monodispersity of the initial nanorod seeds. When increasing CTAB concentration, we consistently achieved a decrease in the aspect ratio of the resulting PT-AuNRs, while maintaining the same average volume per particle. The obtained nanorods featured well-defined pointy tips and lateral facets, maintaining the original pentagonal cross section. These morphological features are attributed to slower gold reduction kinetics due to the stronger surface binding of CTA^{+} and Br^{-}. We additionally found that more extensive overgrowth, achieved by increasing the Au^{3+}/Au^{0} ratio, leads to particles with similar aspect ratios, suggesting a dominating influence of CTAB concentration. Lastly, we demonstrated that this approach can also be applied to other synthetic methods, such as the direct growth of PT-AuNRs from decahedral seeds, thus allowing a fine tuning of AuNR aspect ratio.

Supplementary Materials: The following supporting information can be downloaded at: https://media.sciltp.com/articles/others/2511041613079794/MI-25090103-Supplementary-Materials.pdf.

Author Contributions: F.B.: data curation, visualization, investigation, writing—original draft preparation; L.M.L.-M.: conceptualization, supervision, validation, writing—reviewing and editing. All authors have read and agreed to the published version of the manuscript.

Funding: This work was supported by KU Leuven internal funds (C14/22/085) and by the European Research Council (ERC Synergy Grant no. 101166855, Chiral-Pro). The authors thank Dr. Gail A. Vinnacombe-Willson for her contributions to the organization and editing of the manuscript.

Institutional Review Board Statement: Not applicable.

Data Availability Statement: The data that support the findings of this study are available from the corresponding author upon reasonable request.

Conflicts of Interest: The authors declare no conflict of interest.

Use of AI and AI-assisted Technologies: No AI tools were utilized for this paper.

References

1. Jana, N.R.; Gearheart, L.; Murphy, C.J. Seed-Mediated Growth Approach for Shape-Controlled Synthesis of Spheroidal and Rod-like Gold Nanoparticles Using a Surfactant Template. *Adv. Mater.* **2001**, *13*, 1389–1393.
2. Nikoobakht, B.; El-Sayed, M.A. Preparation and Growth Mechanism of Gold Nanorods (NRs) Using Seed-Mediated Growth Method. *Chem. Mater.* **2003**, *15*, 1957–1962.
3. Scarabelli, L.; Sánchez-Iglesias, A.; Pérez-Juste, J.; Liz-Marzán, L.M. "Tips and Tricks" Practical Guide to the Synthesis of Gold Nanorods. *J. Phys. Chem. Lett.* **2015**, *6*, 4270–4279.
4. Sánchez-Iglesias, A.; Winckelmans, N.; Bals, S.; Grzelczak, M.; Liz-Marzán, L.M. High Yield Seeded Growth of Monodisperse Pentatwinned Gold Nanoparticles Through Thermally-Induced Seed Twinning. *J. Am. Chem. Soc.* **2017**, *139*, 107–110.

5. González-Rubio, G.; Kumar, V.; Llombart, P.; Díaz-Núñez, P.; Bladt, E.; Altantzis, T.; Bals, S.; Peña-Rodríguez, O.; Noya, E.G.; MacDowell, L.G.; et al. Disconnecting Symmetry Breaking from Seeded Growth for the Reproducible Synthesis of High Quality Gold Nanorods. *ACS Nano* **2019**, *13*, 4424–4435.
6. Huang, X.; El-Sayed, I.H.; El-Sayed, M.A. In *Cancer Nanotechnology*; Humana Press: Totowa, NJ, USA, 2010; pp. 343–357.
7. Langer, J.; De Aberasturi, D.J.; Aizpurua, J.; Alvarez-Puebla, R.A.; Auguié, B.; Baumberg, J.J.; Bazan, G.C.; Bell, S.E.J.; Boisen, A.; Brolo, A.G.; et al. Present and Future of Surface-Enhanced Raman Scattering. *ACS Nano* **2020**, *14*, 28–117.
8. Troncoso-Afonso, L.; Vinnacombe-Willson, G.A.; García-Astrain, C.; Liz-Márzan, L.M. SERS in 3D Cell Models: A Powerful Tool in Cancer Research. *Chem. Soc. Rev.* **2024**, *53*, 5118–5148.
9. Canbek, Z.C.; Cortes-Huerto, R.; Testard, F.; Spalla, O.; Moldovan, S.; Ersen, O.; Wisnet, A.; Wang, G.; Goniakowski, J.; Noguera, C.; et al. Twinned Gold Nanoparticles under Growth: Bipyramids Shape Controlled by Environment. *Cryst. Growth Des.* **2015**, *15*, 3637–3644.
10. Hanske, C.; González-Rubio, G.; Hamon, C.; Formentín, P.; Modin, E.; Chuvilin, A.; Guerrero-Martínez, A.; Marsal, L.F.; Liz-Marzán, L.M. Large-Scale Plasmonic Pyramidal Supercrystals via Templated Self-Assembly of Monodisperse Gold Nanospheres. *J. Phys. Chem. C* **2017**, *121*, 10899–10906.
11. González-Rubio, G.; Scarabelli, L.; Guerrero-Martínez, A.; Liz-Marzán, L.M. Surfactant-Assisted Symmetry Breaking in Colloidal Gold Nanocrystal Growth. *ChemNanoMat* **2020**, *6*, 698–707.
12. Jana, N.R.; Gearheart, L.; Murphy, C.J. Wet Chemical Synthesis of High Aspect Ratio Cylindrical Gold Nanorods. *J. Phys. Chem. B* **2001**, *105*, 4065–4067.
13. Chang, H.-H.; Murphy, C.J. Mini Gold Nanorods with Tunable Plasmonic Peaks beyond 1000 Nm. *Chem. Mater.* **2018**, *30*, 1427–1435.
14. González-Rubio, G.; Llombart, P.; Zhou, J.; Geiss, H.; Peña-Rodríguez, O.; Gai, H.; Ni, B.; Rosenberg, R.; Cölfen, H. Revisiting the Role of Seed Size for the Synthesis of Highly Uniform Sub-10 nm Length Gold Nanorods. *Chem. Mater.* **2024**, *36*, 1982–1997.
15. Harper-Harris, J.; Kant, K.; Singh, G. Oleic Acid-Assisted Synthesis of Tunable High-Aspect-Ratio Multiply-Twinned Gold Nanorods for Bioimaging. *ACS Appl. Nano Mater.* **2021**, *4*, 3325–3330.
16. Wu, H.-Y.; Chu, H.-C.; Kuo, T.-J.; Kuo, C.-L.; Huang, M.H. Seed-Mediated Synthesis of High Aspect Ratio Gold Nanorods with Nitric Acid. *Chem. Mater.* **2005**, *17*, 6447–6451.
17. Almora-Barrios, N.; Novell-Leruth, G.; Whiting, P.; Liz-Marzán, L.M.; López, N. Theoretical Description of the Role of Halides, Silver, and Surfactants on the Structure of Gold Nanorods. *Nano Lett.* **2014**, *14*, 871–875.
18. Meena, S.K.; Sulpizi, M. Understanding the Microscopic Origin of Gold Nanoparticle Anisotropic Growth from Molecular Dynamics Simulations. *Langmuir* **2013**, *29*, 14954–14961.
19. Gómez-Graña, S.; Hubert, F.; Testard, F.; Guerrero-Martínez, A.; Grillo, I.; Liz-Marzán, L.M.; Spalla, O. Surfactant (Bi)Layers on Gold Nanorods. *Langmuir* **2012**, *28*, 1453–1459.
20. Zech, T.; Schmutzler, T.; Noll, D.M.; Appavou, M.-S.; Unruh, T. Effect of Bromide on the Surfactant Stabilization Layer Density of Gold Nanorods. *Langmuir* **2022**, *38*, 2227–2237.
21. Mosquera, J.; Wang, D.; Bals, S.; Liz-Marzán, L.M. Surfactant Layers on Gold Nanorods. *Acc. Chem. Res.* **2023**, *56*, 1204–1212.
22. González-Rubio, G.; Díaz-Núñez, P.; Rivera, A.; Prada, A.; Tardajos, G.; González-Izquierdo, J.; Bañares, L.; Llombart, P.; Macdowell, L.G.; Palafox, M.A.; et al. Femtosecond Laser Reshaping Yields Gold Nanorods with Ultranarrow Surface Plasmon Resonances. *Science* **2017**, *358*, 640–644.
23. Meena, S.K.; Celiksoy, S.; Schäfer, P.; Henkel, A.; Sönnichsen, C.; Sulpizi, M. The Role of Halide Ions in the Anisotropic Growth of Gold Nanoparticles: A Microscopic, Atomistic Perspective. *Phys. Chem. Chem. Phys.* **2016**, *18*, 13246–13254.
24. Sánchez-Iglesias, A.; Jenkinson, K.; Bals, S.; Liz-Marzán, L.M. Kinetic Regulation of the Synthesis of Pentatwinned Gold Nanorods below Room Temperature. *J. Phys. Chem. C* **2021**, *125*, 23937–23944.
25. Bevilacqua, F.; Girod, R.; Martín, V.F.; Obelleiro-Liz, M.; Vinnacombe-Willson, G.A.; Van Gordon, K.; Hofkens, J.; Taboada, J.M.; Bals, S.; Liz-Marzán, L.M. Additive-Free Synthesis of (Chiral) Gold Bipyramids from Pentatwinned Nanorods. *ACS Mater. Lett.* **2024**, *6*, 5163–5169.
26. Pérez-Juste, J.; Pastoriza-Santos, I.; Liz-Marzán, L.M.; Mulvaney, P. Gold Nanorods: Synthesis, Characterization and Applications. *Coord. Chem. Rev.* **2005**, *249*, 1870–1901.
27. Yu, R.; Liz-Marzán, L.M.; De Abajo, F.J.G. Universal Analytical Modeling of Plasmonic Nanoparticles. *Chem. Soc. Rev.* **2017**, *46*, 6710–6724.
28. Rangel, T.; Kecik, D.; Trevisanutto, P.E.; Rignanese, G.-M.; Van Swygenhoven, H.; Olevano, V. Band Structure of Gold from Many-Body Perturbation Theory. *Phys. Rev. B* **2012**, *86*, 125125.
29. Hendel, T.; Wuithschick, M.; Kettemann, F.; Birnbaum, A.; Rademann, K.; Polte, J. In Situ Determination of Colloidal Gold Concentrations with UV–Vis Spectroscopy: Limitations and Perspectives. *Anal. Chem.* **2014**, *86*, 11115–11124.